Liquid Crystals
Publication details, including instructions for authors and subscription information:
http://www.informaworld.com/smpp/title~content=t713926090

Synthesis and characterization of new ferroelectric liquid crystals containing a phenyl biphenyl carboxylate mesogenic group and oligooxyethylene spacers

Ging-Ho Hsiue[a][b]; Jung-Lung Wu[a]; Jr-Hong Chen[a]
[a] Department of Chemical Engineering, National Tsing Hua University, Hsinchu, Taiwan, R.O.C. [b] Department of Chemical Engineering, National Chung Hsing University, Taichung, Taiwan, R.O.C.

To cite this Article Hsiue, Ging-Ho , Wu, Jung-Lung and Chen, Jr-Hong(1996) 'Synthesis and characterization of new ferroelectric liquid crystals containing a phenyl biphenyl carboxylate mesogenic group and oligooxyethylene spacers', Liquid Crystals, 21: 4, 449 — 459

To link to this Article: DOI: 10.1080/02678299608032854

URL: http://dx.doi.org/10.1080/02678299608032854

LIQUID CRYSTALS, 1996, VOL. 21, NO. 4, 449–459

Synthesis and characterization of new ferroelectric liquid crystals containing a phenyl biphenyl carboxylate mesogenic group and oligooxyethylene spacers

by GING-HO HSIUE*†‡, JUNG-LUNG WU† and JR-HONG CHEN†

†Department of Chemical Engineering, National Tsing Hua University, Hsinchu,
Taiwan, R.O.C.

‡Department of Chemical Engineering, National Chung Hsing University,
Taichung, Taiwan, R.O.C.

(*Received 22 November 1995; in final form 13 March 1996; accepted 13 March 1996*)

Two series of ferroelectric liquid crystals containing a phenyl biphenyl carboxylate mesogenic group and oligooxyethylene spacers were synthesized. The mesomorphic behaviours of the compounds were characterized using differential scanning calorimetry (DSC), optical polarizing microscopy (POM) and powder X-ray diffraction measurements. These series all contain a smectic A (S_A), a chiral smectic C (S_C^*) and a crystal E (Cr E) phase sequence. The ordered smectic Cr E phase was observed for the short spacer chain ($n=0$, 1, 2) homologues of the two series. Moreover, the mesomorphic properties are discussed as a function of the oligooxyethylene spacer length, and the position of the aromatic core rings. These results indicate that the structures with a rigid part (biphenyl group) closer to the flexible spacer chain (oxyethylene unit) tend to form the symmetrical smectic S_A and Cr E phases.

1. Introduction

Ferroelectric liquid crystals (FLCs) [1–3] and ferroelectric liquid crystalline polymers (FLCPs) are studied extensively for display applications [4–8]. A FLC material used for a display should exhibit a smectic phase over a wide temperature range, including room temperature [9]. Moreover, the liquid crystal material must possess a large spontaneous polarization. As a result, a FLC related device can be operated at a reduced driving voltage. These properties are influenced by the molecular structures of the liquid crystal compounds. Consequently, it is of interest to synthesize ferroelectric liquid crystal compounds which exhibit favourable spontaneous polarization values and smectic characteristics over a wide temperature range, especially room temperature. Besides low molar mass FLCs, several side chain liquid crystalline polymers (LCPs) exhibiting a chiral smectic C mesophase have been reported [10–13]. Ferroelectric properties, for example, spontaneous polarization in these polymers, have also been provided in some cases [10–13]. As a part of our research to develop high efficiency FLC materials, we have designed and synthesized some novel low molar mass FLCs and ferroelectric side chain liquid crystalline polymers [14–21]. They possess a broad temperature range chiral smectic C phase and satisfactory electro-optical properties [17].

In our previous work, a series of FLCs was synthesized and characterized [14].

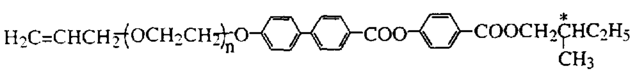

(n= 0, 1, 2, 3)

These compounds have excellent smectic characteristics, especially the chiral smectic C phase, over a wide temperature range and near room temperature. In this study, two new series of FLCs are synthesized and characterized. These novel materials contain the oligooxyethylene spacer, a phenyl biphenyl carboxylate mesogenic group, and various chiral moieties, including (*R*)-1-methylheptoxycarbonyl and (2*S*,3*S*)-2-chloro-3-methylpentanoyloxy groups. The influence of the spacer units and the different chiral tails on the formation of mesophases is also discussed.

The new series have the general formulae:

Series I

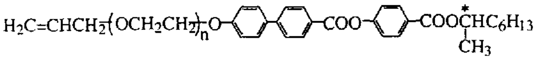

MD*n*21B (n= 0, 1, 2, 3)

Series II

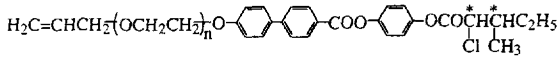

MD*n*21C (n= 0, 1, 2, 3)

---

*Author for correspondence.

2. Synthesis

The compounds of series MD*n*21B, and MD*n*21C were prepared as shown in the Scheme. A detailed synthesis is described in the Experimental Section.

3. Results and discussion

Tables 1 and 2, and figures 1(*a*) and (*b*) show the phase sequences and transition temperatures for the new series MD*n*21B and MD*n*21C.

3.1. *Optical microscopy*

3.1.1. *Series MDn21B*

The four members of this series contain the (*R*)-1-methylheptyl chiral moiety, an oligooxyethylene spacer chain and a 4-(4-hydroxybiphenyl-4′-carbonyloxy)-benzoate mesogenic group. All the members exhibit a smectic A (S_A) phase. The more ordered smectic Cr E phase was observed for the homologues where $n=0$, 1, 2. On the other hand, the chiral smectic C (S_C^*) phase was found for the homologues with a longer oligooxyethylene spacer ($n=2$, 3). In addition, a twist grain boundary A (TGB_A) phase and a blue phase (BP) are present in MD021B and MD321B, respectively. Upon cooling from the isotropic phase into the S_A phase, a focal-conic texture gradually grew (see figure 2(*a*)). After further cooling from the focal-conic S_A phase, the S_C^* phase appeared as evidenced by the formation of striated lines on the focal-conic fan texture (see figure 2(*b*)) or a broken fan texture (see figure 2(*c*)) due to the different pitch lengths at the various temperatures of the ferroelectric S_C^* phase. By subsequent cooling from the broken fan S_C^* phase, a Cr E phase was observed by the presence of a mosaic texture (see figure 2(*d*)).

The transition temperatures are plotted in figure 1(*a*) as a function of *n*, the number of oxyethylene units. As indicated in this figure, these oxyethylene unit chains significantly depressed the phase transition temperatures. This depression is attributed to the increasing flexibility of the C–O bonds. In addition, the clearing points decreased more than the melting points as the number of oxyethylene units increased, thereby resulting in depressed mesomorphic ranges at longer oxyethylene unit length, similar to the results of our previous work [18, 20]. Moreover, the BP and S_C^* phase ranges increase as the number of oxyethylene units increase. However, the S_A and Cr E phases display an opposite trend.

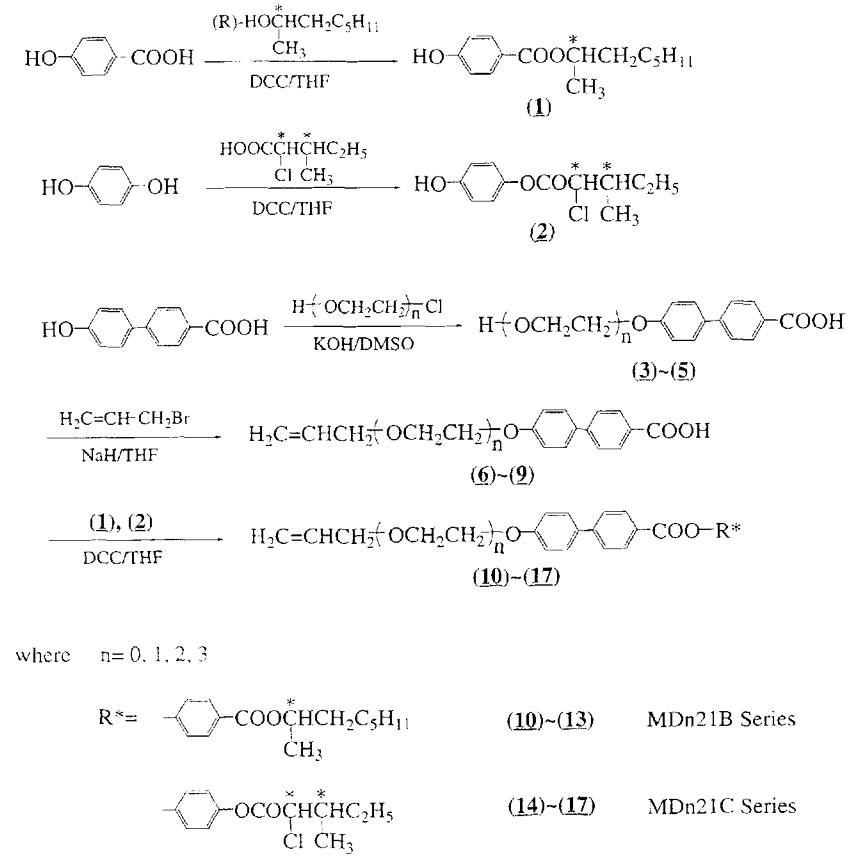

Scheme. The synthesis of ferroelectric liquid crystal series MD*n*21B and MD*n*21C.

Table 1. Transition temperatures for the series MD*n*21B.

Compound	n[a]	Phase transition/°C (corresponding enthalpy changes/mJ mg^{-1})[b]
		Heating Cooling
MD021B	0	Cr 105·4(–) Cr E 109·4(42·4)[c] S_A 162·1(–) TGB_A 162·3(13·4)[d] I
		I 161·2(–) TGB_A 161(10·1)[d] S_A 83·7(–) Cr E 82(44·7)[c] Cr
MD121B	1	Cr 26(7·5) Cr E 87(44·6) S_A 142·5(12·9) I
		I 140·4(13·5) S_A 82·2(12·2) Cr E 24·9(7·7) Cr
MD221B	2	Cr 25(–) Cr E 32·6(11·5)[e] S_C^* 51(–)[f] S_A 93·5(10·5) I
		I 90·8(10·1) S_A 49·6(–)[f] S_C^* 30(–) Cr E 27·4(10·9)[e] Cr
MD321B	3	Cr –0·4(6·8) S 24·7(7·8) S_C^* 30(–) S_A 65·2(5·8) BP 66 I
		I 65·3 BP 64·7(6·0) S_A 28(–) S_C^* 2·6(–) S –3·1(4·1) Cr

[a] n according to scheme.

[b] I = isotropic; Cr E = crystal E; S_C^* = chiral smectic C; S_A = smectic A; TGB_A = twist grain boundary A; BP = blue phase; S = unidentified smectic phase; Cr = crystalline phase.

[c] ΔH(Cr–Cr E–S_A).

[d] ΔH(S_A–TGB_A–I).

[e] ΔH(Cr E–S_C^*–Cr).

[f] Enthalpies were too small to be evaluated.

Table 2. Transition temperatures for the series MD*n*21C.

Compound	n[a]	Phase transition/°C (corresponding enthalpy changes/mJ mg^{-1})[b]
		Heating Cooling
MD021C	0	Cr 49·6(19·5) Cr E 116·3(32·3) S_A 184·4(16·8) I
		I 181·9(11·1) S_A 102·7(11·9) Cr E 52·3(1·5) Cr
MD121C	1	Cr 94(–) Cr E 100·4(12·4)[c] S_A 154·4(9·9) I
		I 150·2(11·3) S_A 97·3(–) Cr E 84·1(12·6)[c] Cr
MD221C	2	Cr 35(–) Cr E 42·6(9·0)[d] S_C^* 80(–)[e] S_A 117·7(7·1) I
		I 116·2(6·7) S_A 72·6(0·6) S_C^* 37·3(–) Cr E 30(8·6)[d] Cr
MD321C	3	Cr 25·5(7·0) S_C^* 45(–)[e] S_A 86·7(6·3) I
		I 84·8(5·2) S_A 42(–)[e] S_C^* 22·5(6·7) Cr

[a] n according to scheme.

[b] I = isotropic; Cr E = crystal E; S_C^* = chiral smectic C; S_A = smectic A; Cr = crystalline phase.

[c] ΔH(Cr–Cr E–S_A).

[d] ΔH(Cr E–S_C^*–Cr).

[e] Enthalpies were too small to be evaluated.

Table 3 compares the mesophase range data of series MD*n*21B with series MD*n*12B ($n = 0$, 1, 2, 3). The two series of compounds contain the same mesogenic core composition (three phenyl rings of an ester core). However, the positions of the phenyl and biphenyl groups differ. The compounds of series MD*n*12B exhibit a rather narrow S_C^* temperature range and have been previously reported [18]. The changing positions of the phenyl and biphenyl groups in the mesogenic cores of MD*n*12B and MD*n*21B result in the following mesomorphic phenomena: (i) the cumulative temperature ranges of the mesophases (ΔT_M) in series MD*n*21B are wider than for the MD*n*12B series; (ii) the increase in the total mesogenic temperature range is dominated by the formation of a Cr E phase, thereby implying that a rigid moiety close to the flexible chain tends to promote the formation of an ordered smectic liquid crystalline mesophase; and (iii) the compounds of series MD*n*21B exhibit the same tendency in forming a narrow S_C^* phase range similar to the series MD*n*12B. These results can

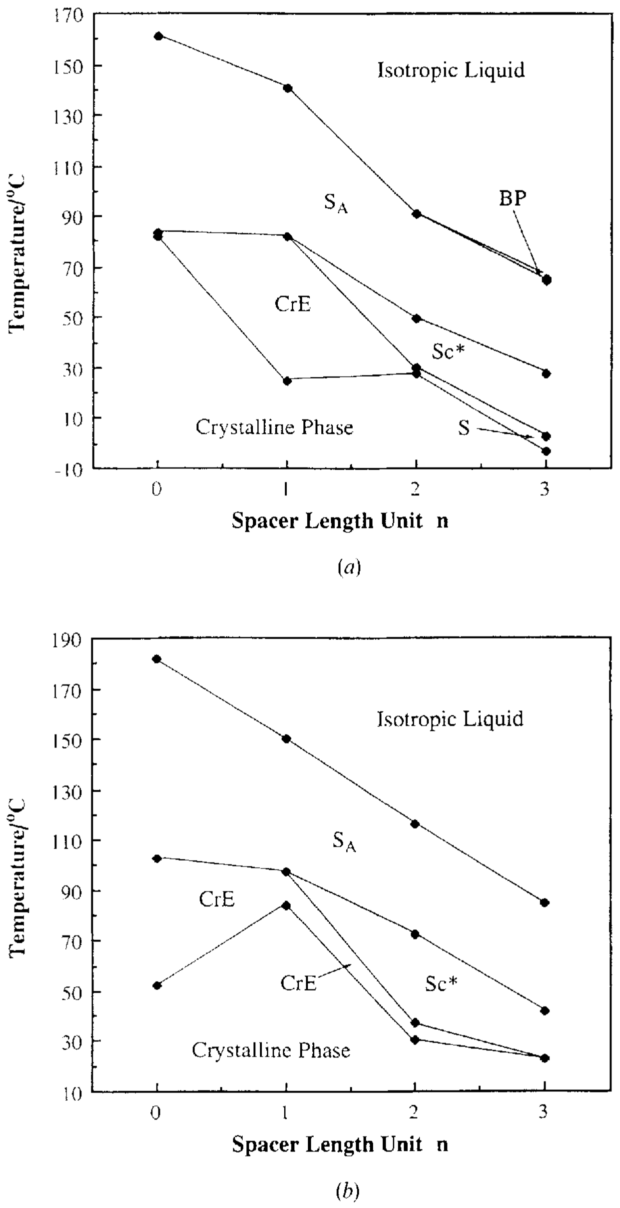

Figure 1. Plots of transition temperatures versus *n*, the number of oxyethylene spacer units (*a*) series MD*n*21B; (*b*) series MD*n*21C.

be accounted for by the fact that the more flexible the chiral tail/oxyethylene spacer system is coupled with a less rigid (three phenyl rings of an ester core) mesogenic group.

3.1.2. *Series MDn21C*

The series of compounds, MD*n*21C, includes the covalently incorporated (2*S*,3*S*)-2-chloro-3-methylpentanoyloxy chiral moiety instead of the (*R*)-1-methyl heptoxycarbonyl group of series MD*n*21B. The four compounds in this series are all mesogenic. Similar to the results of series MD*n*21B, the smectic A phase occurs in all four derivatives. Moreover, the more ordered Cr E phase is present in three (*n* = 0, 1, 2) of the homologues. On the other hand, only the longer homologues (*n* = 2, 3) reveal a S_C^* phase. The optical polarizing microscopy results of the smectic A, chiral smectic C, and Cr E mesophases are the same as the results of series MD*n*21B; a focal-conic fan texture for S_A, striated fans of the S_C^*, and a mosaic texture for the Cr E phase.

Table 4 compares the mesophase ranges of the MD*n*21C and MD*n*12C series. From this table it can be seen that, as with the MD*n*21B and MD*n*12B series, the MD*n*21C series also tends to form the ordered smectic Cr E phase compared to MD*n*12C. Moreover, in changing the positions of the biphenyl and phenyl groups, a widening of the S_A phase for MD*n*21C is observed. However, some of the more disordered liquid crystalline phases disappear, i.e., blue cholesteric and twist grain boundary A phases. These results again imply that rigidity (biphenyl group) close to the flexible spacer chain could promote the formation of the symmetrical smectic phases, the S_A and the Cr E phases. On the other hand, the ΔT_M of MD*n*21C is narrower than the ΔT_M of MD*n*12C owing to the unambiguous supercooling characteristic of MD*n*21C.

3.2. *Calorimetric studies*

Transition enthalpies were determined by differential scanning calorimetry using a Seiko DSC 220C. Tables 1 and 2 list the transition temperatures and corresponding enthalpy values. The thermograms were recorded upon cooling at a rate of 10°C min^{-1} and 5°C (see figures 3(*a*), (*b*) and (*c*)). For MD021B, MD221B, MD321B, MD121C and MD221C, obtaining individual transition enthalpies for the TGB_A/S_A, BP/S_A, S_A/Cr E and S_C^*/Cr E phase transitions proved relatively difficult, due to overlapping. Only the melting transition enthalpies could be determined unambiguously. The tables summarize the enthalpies of some of the overlapping phase transitions.

3.3. *X-ray diffraction investigation*

X-ray diffraction measurements confirmed the presence of the mesophases, S_A, S_C^* and others. Figures 4 and 5 show representative X-ray diffractograms obtained from powder samples of MD221B and MD221C, respectively. Also, curves A–E of figure 4 display a broad reflection at the wide angle (associated with the lateral packing) and a sharp reflection at the small angle (associated with the smectic layers). Curves A and B exhibit rather diffuse reflections at around 4·53 and 4·48 Å, sharp first order reflections at 34·9985 and 35·0167 Å. These results, combined with optical polarizing microscopy observations, confirm the phase as

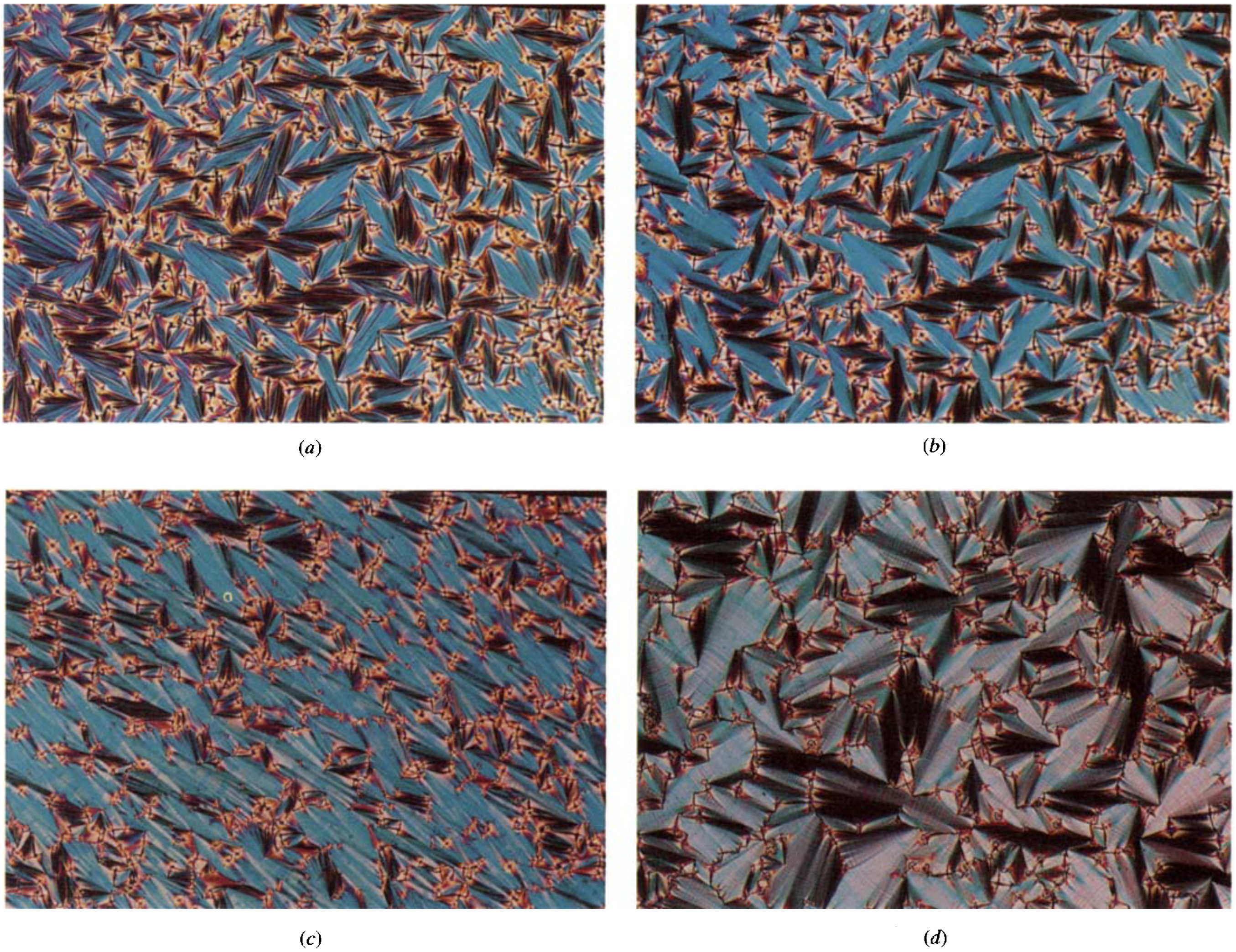

(*a*) (*b*)

(*c*) (*d*)

Figure 2. Optical polarizing micrographs of MD221B ($n=2$): (*a*) the S_a phase at 70°C (400 ×); (*b*) the striated lines on the fan domains of the S_C^* phase at 40°C (400 ×); (*c*) the broken fan texture of the S_C^* phase at 31°C (400 ×); (*d*) the Cr E phase at 29°C (400 ×).

smectic A. Curves C, D and E show a decrease in layer spacing from 34·8976 Å to 34·8302 Å as the temperature decreases from the smectic A phase. This phenomenon is due to the fact that the mesogens' tilt angles generally increase with a decrease in the temperature for the chiral smectic C phase. This is important evidence of the tilted formation of molecules in the ferroelectric S_C^* phase. Also, curves F and G have three sharp reflections at the wide angle, (4·47 Å, 4·05 Å, 3·23 Å) for curve F and (4·46 Å, 4·03 Å, 3·23 Å) for curve G, respectively. Moreover, the sharp first order reflections appear at the small angle, 36·5037 Å for curve F and 36·6037 Å for curve G, respectively. These results correlate sufficiently with the optical polarizing microscopy observation, indicating the Cr E phase [22]. Figure 5 is similar to the results of figure 4: curve A displays a smectic A phase diffraction pattern; curves B–D having a decrease in layer spacing as the temperature decreases reveals a ferroelectric smectic C phase. Moreover, curves E, F reveal the Cr E phase of compound MD221C.

4. Conclusions

Two series of novel ferroelectric liquid crystals containing oligooxyethylene spacers, a phenyl biphenyl carboxylate mesogenic group and different chiral moieties ((*R*)-1-methylheptoxy carbonyl and (2*S*,3*S*)-2-chloro-3-methylpentanoyloxy) were synthesized. All of the compounds exhibit liquid crystalline behaviour. The oxyethylene units as spacer chain favour a lowering of the transition temperatures and depress the mesophases. The MD*n*21B and MD*n*21C series both show Cr E, S_A and S_C^* phases. When compared to the MD*n*12B and

Table 3. Mesophase ranges for the MD*n*21B and MD*n*12B series.

Compound	n	Mesogenic core[a]	ΔT_M[b]	ΔCr E	ΔS_C^*	ΔS_A	ΔTGB_A[d]	ΔCh	ΔBP[d]	Reference
MD021B	0	M_{21}	79·2	1·7	—	77·3	0·2	—	—	[this work]
MD121B	1	M_{21}	115·5	57·3	—	58·2	—	—	—	[this work]
MD221B	2	M_{21}	63·4	2·6	19·6	41·2	—	—	—	[this work]
MD321B	3	M_{21}	68·4	—	25·4	36·7	—	—	0·6	[this work]
MD012B	0	M_{12}	99·8	—	—	99·8	—	—	—	[18]
MD112B	1	M_{12}	77·6	—	3·2	74·4	—	—	—	[18]
MD212B	2	M_{12}	31·7	—	1·3	30·4	—	—	—	[18]
MD312B	3	M_{12}	66·05	—	—[c]	4·32	—	—	—	[18]

[a] M_{21}=

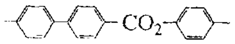

M_{12}=

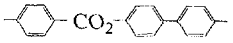

[b] ΔT_M = Total temperature range of mesophase.

[c] The temperature was too low to investigate.

[d] The values were determined by POM.

Table 4. Mesophase ranges for the MD*n*21C and MD*n*12C series.

Compound	n	Mesogenic core[a]	ΔT_M[b]	ΔCr E	ΔS_C^*	ΔS_A	ΔTGB_A[c]	ΔCh	ΔBP[c]	Reference
MD021C	0	M_{21}	129·6	50·4	—	79·2	—	—	—	[this work]
MD121C	1	M_{21}	66·1	13·2	—	52·9	—	—	—	[this work]
MD221C	2	M_{21}	86·2	7·3	35·3	33·6	—	—	—	[this work]
MD321C	3	M_{21}	62·3	—	19·5	42·8	—	—	—	[this work]
MD012C	0	M_{12}	112	—	—	16·8	8·0	85·3	1·5	[18]
MD112C	1	M_{12}	118·3	—	88·2	—	—	23·9	6·2	[18]
MD212C	2	M_{12}	115·9	—	99·8	—	—	4·3	11·8	[18]
MD312C	3	M_{12}	91·9	—	86·73	—	—	—	5·17	[18]

[a] M_{21}=

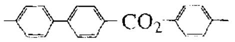

M_{12}=

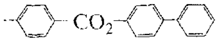

[b] ΔT_M = Total temperature range of mesophase.

[c] The values were determined by POM.

MD*n*12C series (where the biphenyl and phenyl groups change position), results in this study demonstrate that the biphenyl group (rigid part) close to the flexible spacer chains (oxyethylene units) can enhance the thermal stability of the symmetric smectic mesophase, Cr E and S_A phases.

5. Experimental

5.1. *Materials*

4′-Hydroxy-4-biphenylcarboxylic acid, hydroquinone, (*R*)-2-octanol (from TCI), allylbromide, 2-chloroethanol, 2-(2-chloroethoxy) ethanol, 2-(2-(2-chloroethoxy)ethoxy)ethanol (from Aldrich), and other reagents (from Merck) were used as received. The synthesis of (2*S*,3*S*)-2-chloro-3-methylpentanoic acid is given in our previous paper [18].

5.2. *Measurements*

^{1}H NMR spectra were obtained with a Bruker AM300 MHz spectrometer. All spectra were recorded in $CDCl_3$ with TMS as the internal standard unless otherwise noted. A Seiko DSC 220C differential scanning calorimeter equipped with a 5200H computer system was used to determine the thermal transitions, read at the maximum of their endothermic or exothermic peaks. In all cases, heating and cooling rates were 5°C min^{-1}, unless otherwise specified. After the first heating scan, the sample was annealed at 10°C above the isotropization temperature for 5–10 min. Under these conditions, the second heating and cooling scans all recorded reproducible data. The transitions reported were taken during the second or third heating and cooling scans unless otherwise specified. A Nikon Microphot-FX optical

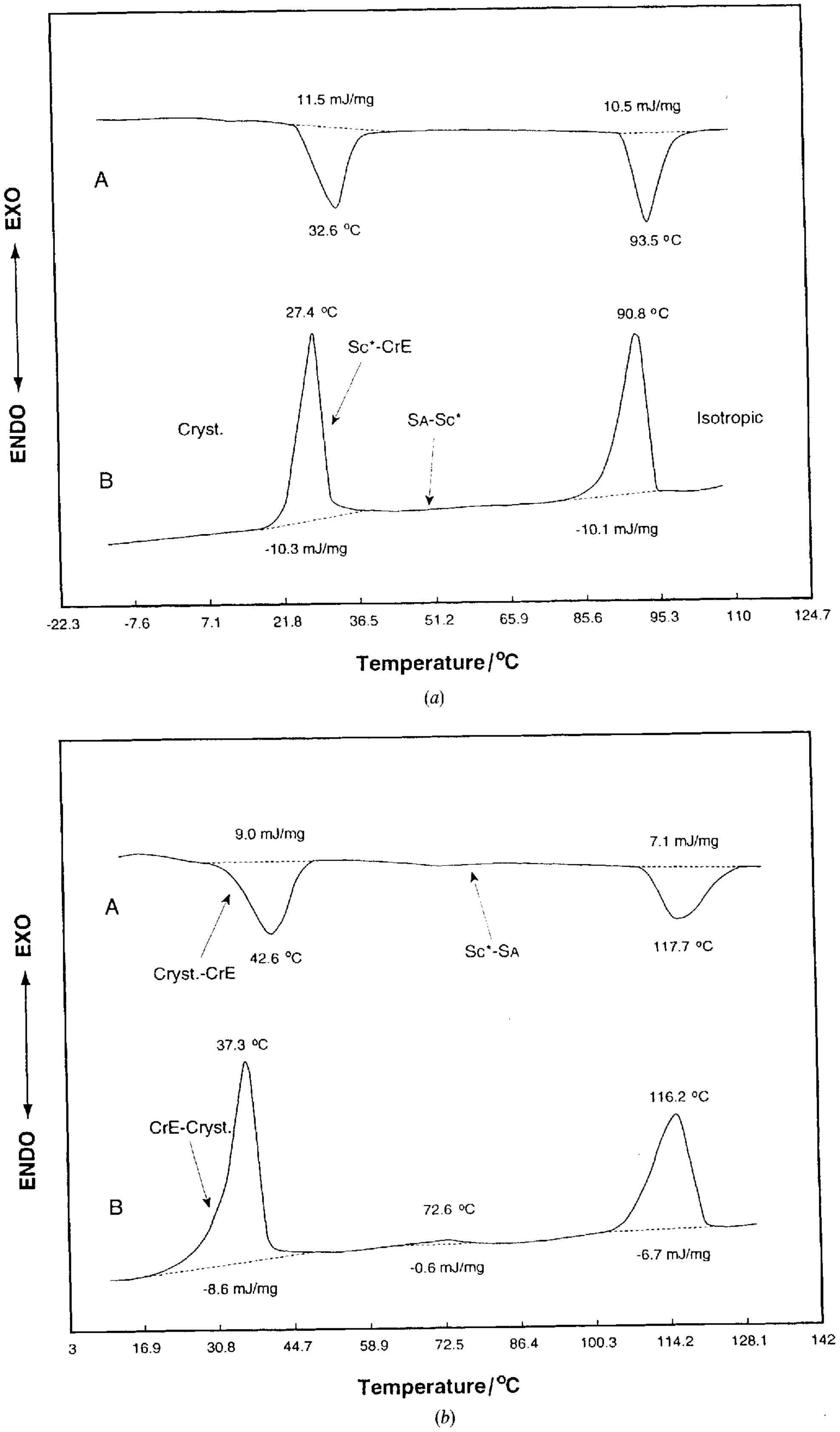

(*a*)

(*b*)

Figure 3. DSC thermograms of (*a*) MD221B (5°C min^{-1}; A. heating scan, B. cooling scan); (*b*) MD221C (5°C min^{-1}; A. heating scan, B. cooling scan).

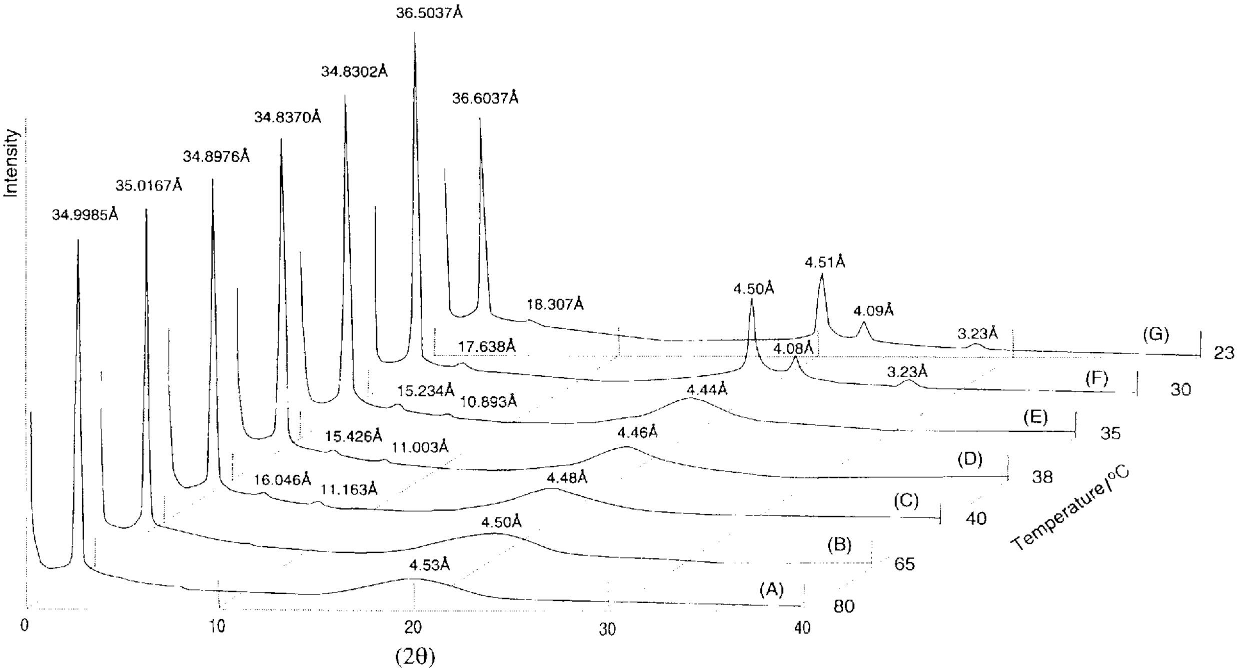

Figure 4. Temperature dependence of powder X-ray diffraction measurements for MD221B at (A) 80, (B) 65, (C) 40, (D) 38, (E) 35, (F) 30, and (G) 23°C.

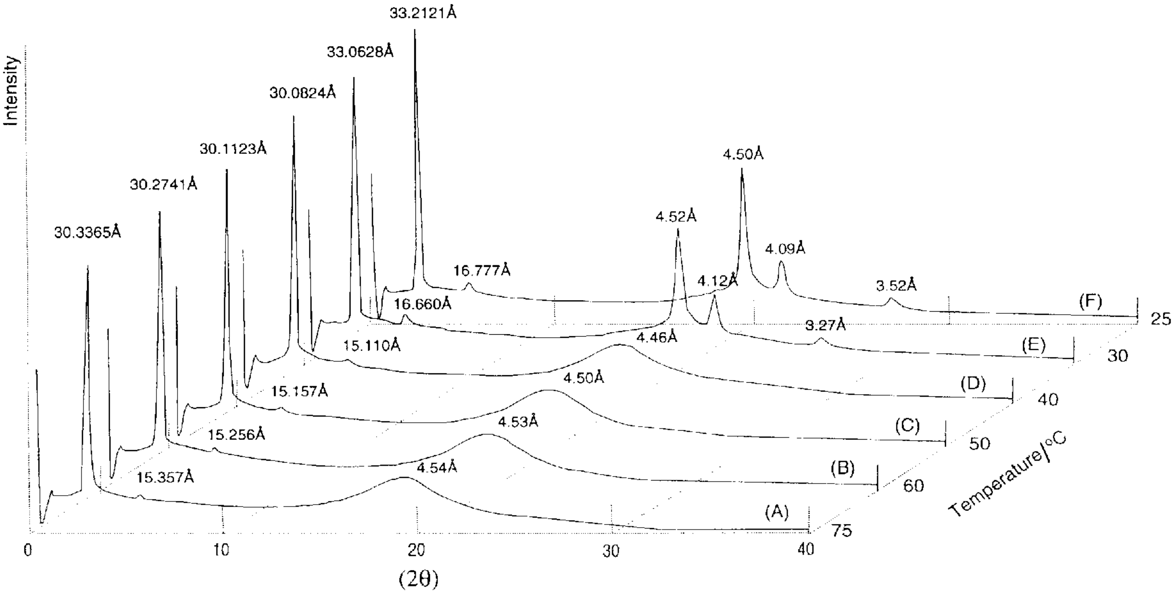

Figure 5. Temperature dependence of powder X-ray diffraction measurements for MD221C at (A) 75, (B) 60, (C) 50, (D) 40, (E) 30, and (F) 25°C.

polarized microscope equipped with a Mettler FP 82 hot stage and a Mettler FP 80 central processor was used to observe the thermal transitions and anisotropic textures. Optical rotations were measured at 25°C on a Jasco DIP-140 digital polarimeter with chloroform as the solvent for all compounds. X-ray diffraction measurements were performed with a Rigaku R-Axis IIC powder diffractometer. Two imaging plate (abbreviated 'IP') detectors were used so that reflection spot exposure and readout operations could be performed. This feature provides increased data collection efficiency and minimizes the time required for IP residual image erasure. The monochromatized X-ray beam from nickel-filtered CuKα radiation with a wavelength of 0·15406 nm was used. A temperature controller was added to the X-ray apparatus for thermal measurements. The precision of the controller was ±0·5°C in the temperature range studied.

5.3. *Synthesis*

5.3.1. *(R)-1-Methylheptyl 4-hydroxybenzoate (**1**) and 4-hydroxyphenyl (2S,3S)-2-chloro-3-methylpentanoate (**2**)*

Compounds **1** and **2** were obtained via similar DCC/THF esterifications; for compound **1**, 4-hydroxybenzoic acid with (*R*)-1-methylheptanol, and for compound **2**, hydroquinone with (2*S*,3*S*)-2-chloro-3-methyl pentanoic acid. In a typical synthesis (for compound **1**): In a 205 ml round bottomed flask, 4-hydroxybenzoic acid, 2·49 g (0·018 mol), (*R*)-1-methylheptanol, 2·59 g (0·0198 mol), DCC 3·734 g (dicyclohexylcarbodiimide) (0·018 mol), 4-pyrrolidino pyridine, 0·444 g (0·003 mol) and dried THF, 50 ml, were stirred under N_2 at 4°C overnight. The solution was filtered and filtrate was washed with 10 per cent HCl(aq) and 5 per cent $NaHCO_3$(aq). The filtrate was then evaporated to yield a yellow oil. The product was purified by flash chromatography (ethyl acetate:hexane = 1:6). Yield: (**1**) 80 per cent; (**2**) 62 per cent. m.p.: (**1**), (**2**) <25°C. ^1H NMR ($CDCl_3$, TMS): (**1**) 0·9 (t, 3 H, $-(CH_2)_4-C\underline{H}_3$), 1·34 (d, 3 H, $-OCHC\underline{H}_3-$), 1·26–2·28 (m, 10 H $-(C\underline{H}_2)_5-CH_3$), 4·44 (m, 1 H, $-O-C\underline{H}CH_3-CH_2-$), 6·9 and 8·05 (2 d, 4 H, aromatic protons). (**2**) 0·9 (t, 3 H, $-CH_2C\underline{H}_3$), 0·97 (d, 3 H, $-CHC\underline{H}_3-C_2H_5$), 1·27 and 1·58 (m, 2 H, $-C\underline{H}_2CH_3$), 2·03 (m, 1 H, $-C\underline{H}CH_3$), 4·14 (m, 1 H, $-C\underline{H}Cl-COO$), 6·9 and 8·05 (2d, 4 H, aromatic protons).

5.3.2. *4-(2-Hydroxyethoxy)-4′-biphenylcarboxylic acid (**3**), 4-(2-(2-hydroxyethoxy)ethoxy)-4′-biphenylcarboxylic acid (**4**), and 4-(2-(2-(2-hydroxyethoxy)ethoxy)ethoxy)-4′-biphenylcarboxylic acid (**5**)*

These compounds were synthesized by the same method. An example synthesis of 4-(2-(2-hydroxyethox-

Table 5. Chemical shift δ and $[\alpha]_d^{25}$ values of the MD*n*21B, and MD*n*21C series.

Monomers	$[\alpha]_d^{25}$ [a]	^1H NMR spectra[b]
MD021B	+27·194	0·9 (t, 3 H, $-(CH_2)_4-C\underline{H}_3$), 1·34 (d, 3 H, $-OCH(C\underline{H}_3)-$), 1·26–2·28 (m, 10 H, $-(C\underline{H}_2)_5-CH_3$), 4·44 (m, 1 H, $-O-C\underline{H}(CH_3)-CH_2-$), 4·6 (m, 2 H, $-C\underline{H}_2-O-$), 5·23 and 5·9 (m, 3 H, $C\underline{H}_2=C\underline{H}-$), 7·0–8·2 (6d, 12 aromatic protons)
MD121B	+25·452	0·9 (t, 3 H, $-(CH_2)_4-C\underline{H}_3$), 1·34 (d, 3 H, $-OCH(C\underline{H}_3)-$), 1·26–2·28 (m, 10 H, $-(C\underline{H}_2)_5-CH_3$), 4·44 (m, 1 H, $-O-C\underline{H}(CH_3)-CH_2-$), 3·81–4·25 (m, 6 H, $-C\underline{H}_2-(OC\underline{H}_2C\underline{H}_2)-$), 5·23 and 5·9 (m, 3 H, $C\underline{H}_2=C\underline{H}-$), 7·0–8·2 (6d, 12 aromatic protons)
MD221B	+22·248	0·9 (t, 3 H, $-(CH_2)_4-C\underline{H}_3$), 1·34 (d, 3 H, $-OCH(C\underline{H}_3)-$), 1·26–2·28 (m, 10 H, $-(C\underline{H}_2)_5-CH_3$), 4·44 (m, 1 H, $-O-C\underline{H}(CH_3)-CH_2-$), 3·81–4·25 (m, 10 H, $-C\underline{H}_2-(OC\underline{H}_2C\underline{H}_2)_2-$), 5·23 and 5·9 (m, 3 H, $C\underline{H}_2=C\underline{H}-$), 7·0–8·2 (6d, 12 aromatic protons)
MD321B	+20·789	0·9 (t, 3 H, $-(CH_2)_4-C\underline{H}_3$), 1·34 (d, 3 H, $-OCH(C\underline{H}_3)-$), 1·26–2·28 (m, 10 H, $-(C\underline{H}_2)_5-CH_3$), 4·44 (m, 1 H, $-O-C\underline{H}(CH_3)-CH_2-$), 3·81–4·25 (m, 14 H, $-C\underline{H}_2-(OC\underline{H}_2C\underline{H}_2)_3-$), 5·23 and 5·9 (m, 3 H, $C\underline{H}_2=C\underline{H}-$), 7·0–8·2 (6d, 12 aromatic protons)
MD021C	−3·212	0·9 (t, 3 H, $-CH_2C\underline{H}_3$), 1·1 (d, 3 H, $-CHC\underline{H}_3-C_2H_5$), 1·4 and 1·7 (m, 2 H, $-C\underline{H}_2CH_3$), 2·2 (m, 1 H, $-C\underline{H}CH_3$), 4·14 (m, 1 H, $-C\underline{H}Cl-COO$), 4·6 (m, 2 H, $-C\underline{H}_2-O-$), 5·23 and 5·9 (m, 3 H, $C\underline{H}_2=C\underline{H}-$), 6·9–8·2 (6d, 12 aromatic protons)
MD121C	−4·415	0·9 (t, 3 H, $-CH_2C\underline{H}_3$), 1·1 (d, 3 H, $-CHC\underline{H}_3-C_2H_5$), 1·4 and 1·7 (m, 2 H, $-C\underline{H}_2CH_3$), 2·2 (m, 1 H, $-C\underline{H}CH_3$), 4·14 (m, 1 H, $-C\underline{H}Cl-COO$), 3·81–4·25 (m, 6 H, $-C\underline{H}_2-(OC\underline{H}_2C\underline{H}_2)-$), 5·23 and 5·9 (m, 3 H, $C\underline{H}_2=C\underline{H}-$), 6·9–8·2 (6d, 12 aromatic protons)
MD221C	−6·523	0·9 (t, 3 H, $-CH_2C\underline{H}_3$), 1·1 (d, 3 H, $-CHC\underline{H}_3-C_2H_5$), 1·4 and 1·7 (m, 2 H, $-C\underline{H}_2CH_3$), 2·2 (m, 1 H, $-C\underline{H}CH_3$), 4·14 (m, 1 H, $-C\underline{H}Cl-COO$), 3·81–4·25 (m, 10 H, $-C\underline{H}_2-(OC\underline{H}_2C\underline{H}_2)_2-$), 5·23 and 5·9 (m, 3 H, $C\underline{H}_2=C\underline{H}-$), 6·9–8·2 (6d, 12 aromatic protons)
MD321C	−5·919	0·9 (t, 3 H, $-CH_2C\underline{H}_3$), 1·1 (d, 3 H, $-CHC\underline{H}_3-C_2H_5$), 1·4 and 1·7 (m, 2 H, $-C\underline{H}_2CH_3$), 2·2 (m, 1 H, $-C\underline{H}CH_3$), 4·14 (m, 1 H, $-C\underline{H}Cl-COO$), 3·81–4·25 (m, 14 H, $-C\underline{H}_2-(OC\underline{H}_2C\underline{H}_2)_3-$), 5·23 and 5·9 (m, 3 H, $C\underline{H}_2=C\underline{H}-$), 6·9–8·2 (6d, 12 aromatic protons)

[a] These values were measured in $CHCl_3$ at 25°C.

[b] These values were measured in $CDCl_3$, using 300 MHz nuclear magnetic resonance spectroscopy (internal standard tetramethylsilane).

y)ethoxy)-4′-biphenylcarboxylic acid (**4**) is given below: A solution of 2-(2-chloroethoxy)ethanol, 3·198 g (0·026 mol) in 5 ml of DMSO (dimethylsulphoxide) was added dropwise to a solution of 4′-hydroxy-4-biphenylcarboxylic acid, 2·5 g (0·012 mol) and powdered potassium hydroxide, 2·088 g (0·037 mol) in 15 ml of DMSO at 70°C. After stirring the reaction mixture under reflux for 24 h, the solution was poured into 300 ml water. The mixture solution was acidified with hydrochloric acid. After cooling to 0°C, a white solid was filtered and set aside. The filtrate was extracted with tetrahydrofuran and the extracted material was evaporated to a white solid which was combined with the set-aside materials. The combined materials (75 per cent yield) was recrystallized from hexane. m.p.: 213°C. ^{1}H NMR (CDCl$_3$, TMS): δ (ppm) = 2·62 (s, 1 H, $-\mathrm{O\underline{H}}$), 3·81–4·25 (m, 8 H, $-(\mathrm{OC\underline{H}_2C\underline{H}_2})_2-$), 6·9, 7·5, 7·6 and 8·1 (4 d, 8 H, aromatic protons), 12·2 (s, 1 H, $-\mathrm{COO\underline{H}}$).

5.3.3. *4-Allyloxy-4′-biphenylcarboxylic acid (**6**), 4-(2-allyloxyethoxy)-4′-biphenylcarboxylic acid (**7**), 4-(2-(2-allyloxyethoxy)ethoxy)-4′-biphenylcarboxylic acid (**8**), and 4-(2-(2-(2-allyloxyethoxy)ethoxy)ethoxy)4′-biphenylcarboxylic acid (**9**)*

These compounds were synthesized by a similar method. An example synthesis of 4-(2-(2-allyloxyethoxy)-ethoxy)-4′-biphenylcarboxylic acid (**8**) is presented below: 4-(2-(2-Hydroxyethoxy)ethoxy)-4′-biphenylcarboxylic acid (**4**), 3 g (0·01 mol) was added to a suspension of 1·91 g (0·079 mol) sodium hydride in 50 ml dried tetrahydrofuran at 4°C. After the hydrogen was completely released, allyl bromide, 3 ml (0·034 mol) was added dropwise to the reaction mixture and then stirred at room temperature overnight. The excess sodium hydride was treated with distilled water and extracted with ethyl acetate. The organic phase was washed with 10 per cent aqueous hydrochloric acid solution, dried over anhydrous magnesium sulphate, and the solvent evaporated on a rotary evaporator. The yellow solid product was purified by recrystallization from hexane with a 72 per cent yield. m.p.: 189·8°C. ^{1}H NMR (CDCl$_3$, TMS): δ (ppm) = 3·81–4·25 (m, 10 H, $-\mathrm{C\underline{H}_2}$-$(\mathrm{OC\underline{H}_2C\underline{H}_2})_2-$), 5·23 and 5·9 (m, 3 H, $\mathrm{C\underline{H}_2{=}C\underline{H}-}$), 6·9, 7·5, 7·6 and 8·1 (4 d, 8 H, aromatic protons), 12·2 (s, 1 H, $-\mathrm{COO\underline{H}}$).

5.3.4. *Series MDn12B: 4-(R)-1-Methyl-l-heptyl [[[4-(allyloxy)]biphenyl-4′-yl]carbonyl]oxy]benzoate (**10**) 4-(R)-1-methyl-1-heptyl[[[4-(2-(allyloxy)ethoxy)]biphenyl-4′-yl]carbonyl]oxy]benzoate (**11**), 4-(R)-1-methyl-1-heptyl[[[4-(2-(2-(allyloxy)ethoxy)ethoxy)]biphenyl-4′-yl]carbonyl]oxy]benzoate (**12**), and 4-(R)-1-methyl-1-heptyl[[[4-(2-(2-(2-(allyloxy)ethoxy)ethoxy)ethoxy)]biphenyl-4′-yl]carbonyl]oxy]benzoate (**13**) Series MDn12C: 4-[(2S,3S)-2-Chloro-3-methylpentanoyloxy]phenyl 4-(allyloxy)biphenyl-4′-carboxylate (**14**), 4-[(2S,3S)-2-chloro-3-methylpentanoyloxy]phenyl 4-[(2-(allyloxy)ethoxy)]biphenyl-4′-carboxylate (**15**), 4-[(2S,3S)-2-chloro-3-methylpentanoyloxy]phenyl 4-[(2-(2-(allyloxy)ethoxy)ethoxy)]biphenyl-4′-carboxylate (**16**), and 4-[(2S,3S)-2-chloro-3-methylpentanoyloxy]phenyl 4-[(2-(2-(2-(allyloxy)ethoxy)ethoxy)ethoxy)] biphenyl-4′-carboxylate (**17**)*

These final products were synthesized by the same method of preparing compounds **1** and **2**. The $[\alpha]_d^{25}$, ^{1}H NMR spectrum are listed in table 5.

The authors would like to thank the National Science Council of the Republic of China (Contact No. NSC-84-2216-E007-029)

References

[1] Meyer, R. B., Liebert, L., Strzelecki, L., and Keller, J. P., 1975, *J. de Phys. Lett.*, **36**, 69.

[2] Clark, N. A., and Largerwall, S. T., 1980, *Appl. Phys. Lett.*, **36**, 898.

[3] Leslie, T. M., 1984, *Ferroelectrics*, **58**, 9.

[4] Furakawa, K., Terashima, K., Ichihashi, M., Inoue, H., Saito, S., and Inukai, T., 1985, 6th Liq. Cryst. Conf. Soc. Count., Halle (GDR), Abstract, A37.

[5] Furakawa, K., and Terashima, K., 1986, European Patent, Application EP 178,647.

[6] Keller, P., 1984, *Mol. Cryst. liq. Cryst.*, **102**, 295.

[7] Koden, M., Katsuse, H., Itoh, N., Kaneko, T., Tamai, K., Takeda, H., Shiomi, M., Numao, N., Kido, M., Matsuki, M., Miyoshi, S., and Wada, T., 1993, Fourth International Conference on Ferroelectric Liquid Crystals, Abstract p-146, p. 369.

[8] Tajima, E., Kondoh, S., and Suzuki, Y., 1993, Fourth International Conference on Ferroelectric Liquid Crystals, Abstract p-147, p. 371.

[9] Adams, T. G., and Sinta, R., 1989, *Mol. Cryst. liq. Cryst.*, **177**, 145.

[10] Scherowsky, G., Schliwa, A., Springer, J., Kuhnpast, K., and Trapp, W., 1989, *Liq. Cryst.*, **5**, 1281.

[11] Shibaev, V. P., Kozlovsky, M. V., and Plate, N. A., 1990, *Liq. Cryst.*, **8**, 1281.

[12] Vallerien, S. U., Kremer, F., and Fischer, E. W., 1990, *Makromol. Chem., rap. Commun.*, **11**, 593.

[13] Kapizta, H., and Zentel, R., 1991, *Makromol. Chem.*, **192**, 1859.

[14] Hsu, C. S., Shih, L. J., and Hsiue, G. H., 1993, *Macromolecules*, **26**, 3161.

[15] Chen, J. H., Chang, R. C., and Hsiue, G. H., 1993, *Ferroelectrics*, **147,** 241.

[16] Hsiue, G. H., and Chen, J. H., 1995, *Macromolecules*, **28,** 4366.

[17] Wu, S. L., Hsieh, W. J., Chen, D. G., Chen, S. J., Shyu, J. T., and Hsiue, G. H., 1995, *Mol. Cryst. liq. Cryst.*, **265,** 39.

[18] Chen, J. H., Chang, R. C., Guu, F. W., Hsiue, G. H., and Wu, S. L., 1995, *Liq. Cryst.*, **18,** 291.

[19] Hsiue, G. H., Lee, G. R., and Chen, J. H., 1995, *Macromol. chem. Phys.*, **196,** 2601.

[20] Chen, J. H., Hsiue, G. H., Hwang, C. P., and Wu, J. L., 1995, *Liq. Cryst.*, (in the press).

[21] Hsiue, G. H., Hwang, C. P., and Chen, J. H., 1995, *Liq. Cryst.*, (in the press).

[22] Doucet, J., Levelut, A. M., Lambert, M., Liebert, L., and Strzeleck, L., 1975, *J. Phys. Colloq.*, **36,** C1-13.